Effect of Orientation on Two-phase Slug Flow Induced Vibrations

Huzaifa Azam[1], William Pao[1,*], Muhammad Sohail[1], Umair Khan[1]

[1] Mechanical Engineering Department, Universiti Teknologi PETRONAS (UTP), Seri Iskandar 32610, Malaysia

ARTICLE INFO	ABSTRACT
	Multiphase flow induced vibrations is a serious safety issue in oil and gas industries due to its undesirable vibration. Currently, there is a lack of usable data that could help to predict the magnitude of multiphase flow induced vibration in pipe inclined at various angles. The objective of this paper is to determine the magnitude of vibration in two-phase flow in pipe at inclination angle of 0°, 30°, 45°, 60°, and 90°. Air to water superficial velocity ratio of 1.25 was selected for this purpose because it is the value that causes the flow to change abruptly from slug to churn flow and vice versa, depending on the orientation angle. The flow conduit is selected to be a stainless-steel pipe with an internal diameter of 52.5 mm (2 inches). The vibrations are monitored at the pipe section of length 38D from the inlet. Maximum longitudinal vibrations were observed in 0° orientation. 60° encountered the maximum amplitude vibrational frequency in transverse direction but being at a higher frequency. The suggested model can be used to evaluate the FSI impact of unstable vibrations for any piping orientation and diameter.

1. Introduction

Fluid-structure interaction (FSI) has gained immense attention in recent years due to increasing requirement for industries to deliver large quantities of liquid mixture from one place to another in the cheapest possible way. Multiphase flow induced structural vibration creates undesirable structural fatigue and other downstream production related issues, leading to serious shortcoming in safety and sustainability. Zheng *et al.,* [1] observed that the flow-induced vibrations were dominated by the gas phase, leading to significant structural deformation. Furthermore, they found that the gas-solid interaction had a significant impact on the fluid's behaviour and structural response. Ruojun *et al.,* [2] discussed fluid structure interaction in internal two-phase flow via production pipes, in which fluid pressures are communicated to the pipe wall and, conversely, structural deformation represented by displacement is conveyed back to the fluid domain.

Wang *et al.,* [3] showed that slug flow is the most challenging phenomenon among all internal two-phase flows in a pipeline because of its flow instability and local phase fluctuations. Additional parameters include fluctuations in pressure, individual phase densities, and superficial velocities

---

* Corresponding author.
E-mail address: william.pao@utp.edu.my

contributing to the overall momentum flux fluctuations. Resonance may be produced due to the proximity of the excitation force frequency and the piping natural frequency in the presence of such fluctuations. Yih and Griffith [4] measured the impacting force when two-phase fluids hit a "turning tee." The experiment was conducted on a tee shape phase separator piping arrangement and significant vibrations were obtained. Smaller duct diameters of range 6.35mm, 15.9mm and 25.4mm were investigated with a velocity range of 15-75m/s. The volume fraction of gas was taken between 50-100%. It was observed that the maximum void fraction fluctuations were high in slug and annular flows. The observed frequency was less than 30 Hz. They concluded that flow velocity is closely related to low-frequency oscillation of the momentum fluxes, which can be significant. Whenever two-phase flow passes through pipe, unstable forces are produced due to the flow regimes and superficial velocities. These results were discussed by Riverin *et al.,* [5] and Riverin and Pettigrew [6]. Wang *et al.,* [3] carried out an experimental examination on a small piping system with two elbows, straight sections, and a U-shaped configuration that was subjected to internal two-phase air-water flow. The findings show that the periodic momentum flux variations of the air-water flow and the first modes of piping system vibration resonance phenomenon was the primary source of pipe vibration. As a result, the predominant frequency of the excitation force increased proportionally as the mixture velocity increased.

Tay and Thorpe [7] conducted experiments on a horizontal 90-degree pipe bend to investigate the effect of density, viscosity and surface tension on slug flow induced stresses. The liquid and gas superficial velocities used for experiment were 0.38 – 2.87 m/s and 0.2 – 0.7 m/s, respectively. A 70mm internal diameter pipe was used in the experiment. Void fraction was observed to be increasing with reducing the liquid surface tension, however, it was concluded that viscosity had very limited impact on the liquid holdup. The greatest resultant force predicted by PFM and its square root revealed a linear connection with mixture velocity. The study concluded that the force characteristics were not significantly affected by the physical qualities of the liquid. Cargnelutti *et al.,* [8] tested the stratified, slug, and annular flows in horizontally oriented pipes with an internal diameter of 25.4 mm. The surface velocities of the gas and liquid were 0.1 to 30 m/s and 0.05 to 2 m/s, respectively. Forces were measured for straight pipes, T-joints, T-joints with one of the arms closed off (T-bends), and two 90^0 bends with 1-inch internal diameter, having R/D ratio of 1 and 2 each. The values predicted by Riverin *et al.,* [5] model and the measured dimensionless slug flow-induced forces in the bend and T-bend were in good agreement. The stratified and annular flows data, however, did not match the Riverin *et al.,* [5] model.

Li *et al.,* [9] studied air-water multiphase flow in a M-shaped jumper for a mixture velocity range of 1 m/s to 4 m/s and water volume fractions of 0.2 and 0.8. The aim of this study was to determine the relationship between the flow patterns and their contribution to flow induced vibrations. The generation of Taylor bubbles and their regularity in the first ascending segment is focussed. A consistent decrease in pressure was observed as fluid mixture was transported from the ascending segment from the inlet to outlet. Maximum deformation and directional stresses were observed at elbows.

Wang *et al.,* [10] numerically investigated the fluid structure interaction in horizontal pipe. Maximum pipe deformation and equivalent stress of 1.8 mm and 7.5 MPa was observed under the stratified flow conditions. Periodic fluctuations were observed by the dynamic responses of slug, wavy and annular flows. A maximum pipe deformation of 4mm and equivalent stress of 17.5 MPa was obtained under the slug flow conditions.

High safety standards are necessary for calculations with fluid-structure interaction, which are typically seen in nuclear and chemical industries. They may also be helpful for troubleshooting, developing design standards, and post-accident analyses [11-13]. Currently available literature states

inadequate information regarding the vibrational properties induced by slug, annular and stratified flows for various orientation of a pipe. Whereas focus of parametric two-phase flow induced vibration studies have been the influence of superficial velocities on flow induced vibrations. The goal of this research is to increase understanding of high-frequency vibrations in straight pipe inclined at different orientations and to provide an approach to simulate such piping systems. By monitoring the induced vibration of a pipe segment in the simulated flow, various flow rates of air/water can be simulated using the similar methodology. The vibration of the pipeline is studied in relation to the impact of water and air superficial velocities, and the amplitudes and frequencies of the pipeline are calculated.

2. Methodology
2.1 Geometry

The geometry used has a length equal to 81D where D is the internal diameter of the pipe i.e. 0.0525m (2 inches). A thickness of 5 mm was utilized for pipe structure model geometry. The pipe inlet cross section is divided into water and air inlets to separately introduce the inlet velocities. The displacement and pressure fluctuation readings were recorded at 75D distance from the pipe inlet for 10 s after flow is fully developed and system is statistically converged.

2.2 Flow Modelling

The slug flow was modelled for five different orientations by holding the inlet superficial velocities constant for a 52.5 mm internal diameter horizontal pipe. Various flow regimes are studied in the literature for this diameter horizontal orientation. Impact of orientations on flow structure interaction was studied from horizontal 0° to vertical 90° in this study by changing gravitational acceleration components along x and y-axis shown in Figure 1. Slug flow velocities were selected from Baker's flow regime map. When the pipe is oriented at different angles, the back flow and turbulent viscosity becomes dominant. To encounter that backflow and turbulent viscosities the courant number is changed continuously. Courant number is taken less than 0.5 for this study. Wang *et al.,* [10] simulated the mentioned air-water two-phase flow regimes using volume of fluid model and k-ε turbulence model. Similar model was used in the present study.
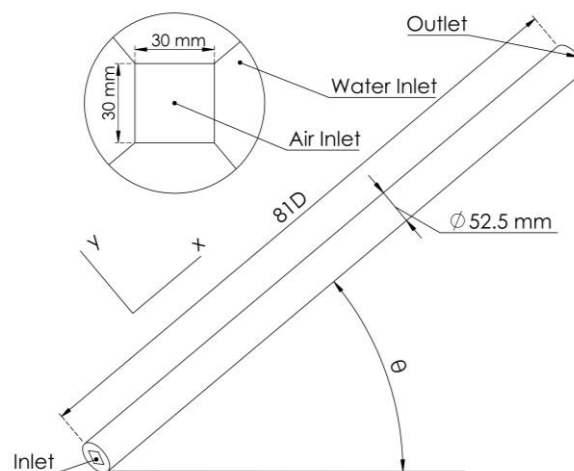
Fig. 1. Pipe geometry

2.2.1 Boundary conditions

Boundaries for this study are inlet, outlet, and fluid wall. Outer surface of fluid geometry is interfaced with the inner surface of pipe structural geometry. This interface transfers of fluid forces to structure inner surface and structure displacement to fluid for a fully coupled fluid structure interaction model. For this study, superficial velocities with a void fraction of 0.5 in the flow channel were chosen. Based on the inlet surface area ratio presented in Figure 1, the inlet velocities of air and water were calculated for void fraction of 0.5 and set to 15.7 m/s and 12.9 m/s, respectively. Standard atmospheric pressure (101.3 KPa) and 25°C were listed as the operating conditions. The gravitational effect is considered and is pointing downwards at 6 o'clock direction. Piper structure in transient structure model was having 2 fixed supports, one at each end.

2.2.2 Multi-phase model

Incompressible two-phase flow model incorporating the Volume of Fluid (VOF) method for capturing phase interfaces along with k-ε turbulence model is considered [9]. VOF model captures the interface between phases using interface tracking method. According to Kvicinsky *et al.,* [14], this powerful tool makes it possible to simulate complex free surface flows with any shape and boundary conditions. The modelling conditions for simulating slug flow at different orientations are given in Table 1.

Table 1
Modelling conditions for CFD

Case	Orientation	Diameter (mm)	Superficial Velocity of Air (m/s)	Superficial Velocity of Water (m/s)	Flow Modeled
1	0	52.5	15.9	12.7	Slug
2	30	52.5	15.9	12.7	Slug/Dispersed bubbles
3	45	52.5	15.9	12.7	Slug/Bubbly flow
4	60	52.5	15.9	12.7	Slug
5	90	52.5	15.9	12.7	Slug/Annular

2.3 Data Collection

The flow chart of the simulation process is shown in Figure 2. FSI model is validated against the flow regimes of slug and annular flow with the assistance of flow contours and then the structural displacements and pressure fluctuations are recorded against the simulated time at 75D from the inlet. Fast Fourier transforms are used to find out the peak frequencies. Both fluid and pipe structures are coupled for fluid forces and structure displacement data sharing at fluid solid interface surface. CFD employs Volume of Fluid (VOF) method for multi-phase flow simulation modelling of slug and related flow patterns, aligning with the corresponding phasal velocities. This method was introduced by Nichols and Hirt [15] and was further studied by Hirt and Nichols [16]. They described the governing equations employed by the VOF approach and the void fraction continuity equation used to calculate the occupancy of the phases in the flow. The k-model is usually employed in a range of industrial applications and piping layouts for the turbulence modelling for different diameters and orientations of pipe. These models were introduced by Launder [17]. By employing ANSYS's System Coupling component at the Project Schematic level, two-way coupling is employed to connect the two solvers for FSI simulations. The inner diameter and entrance (Pipe) length, L_{IN}, are the major factors that determine the pipe vibrations and stresses.
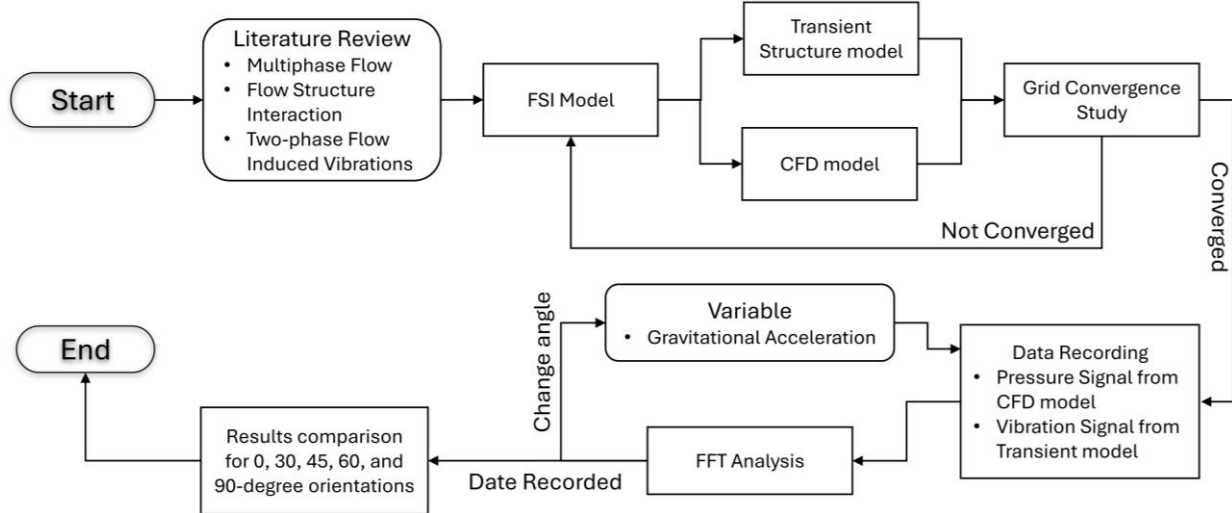
Fig. 2. Flow chart of the simulation process for simulation validation and FSI study

2.4 Governing Equations

The governing equations of two-phase flow are discussed in two sub sections; that include pipe structure, two-phase flow, and the coupling between structure and fluid flow. The problems under consideration consist of a fluid that is occupying a given domain Ω^F and a structure that occupies another domain Ω^s which interact at the common boundary T [18].

2.4.1 Structural equations

Structural displacements produced are governed by the following Eq. (1).

$$\rho^S \frac{D^2 u}{Dt^2} - \nabla.\left(\boldsymbol{F}.\boldsymbol{S}(u)\right) = \rho^S \boldsymbol{b^s} \qquad \text{in } \Omega^s \times (0, T) \tag{1}$$

Structural displacements, body forces, Piola-Kirchhoff stress tensor, density of structure and deformation gradient tensor are represented by u, $\boldsymbol{b^s}$, **S**, ρ^s, **F** respectively.

2.4.2 Fluid flow equations

Navier-Stokes equations for incompressible fluids expressed in Arbitrary Lagrangian-Eulerian (ALE) framework are to be solved [19]. Taking fluid as viscus identity, equations for fluid flow are derived from the law of conservation of mass and conservation of momentum [20].

$$\rho^F \frac{dv}{dt}\bigg|_{x}, + \rho^F.\boldsymbol{c}.\nabla\boldsymbol{v} - 2\mu\nabla.\boldsymbol{\varepsilon}(\boldsymbol{v}) + \nabla\bar{\rho} = \rho^F \boldsymbol{b^F} \qquad \text{in } \Omega^F \times (0, T) \tag{2}$$

$$\nabla.\boldsymbol{v} = 0 \qquad \text{in } \Omega^F \times (0, T) \tag{3}$$

Here $\boldsymbol{v}$ denotes the fluid velocity while physical pressure is given by $\bar{\rho}$. Density and viscosity of the fluid are denoted by ρ^F and μ respectively. Forces applied by fluid body are represented by $\boldsymbol{b^F}$ and strain rate tensor is given by $\boldsymbol{\varepsilon}(\boldsymbol{v})$. Eq. (2) depicts the fluid acceleration and convective terms in the ALE formulation.

2.4.3 Coupling equations

Kinematic and dynamic continuity is achieved at the interface Γ. The kinematic coupling governing equations for the fluid body and structure are shown in Eq. (3).

$$u_{\Gamma}(t) = d^{F}_{\Gamma}(t), \qquad \dot{u}_{\Gamma}(t) = v_{\Gamma}(t), \qquad \ddot{u}_{\Gamma}(t) = v_{\Gamma}(t) \qquad (4)$$

Here $d^{F}_{\Gamma}(t)$ Displacements of the fluid mesh nodes at fluid solid interface is given by $d^{F}_{\Gamma}(t)$. Concluding form for the dynamic coupling equation is shown in Eq. (4).

$$h^{s}(t) + h^{F}(t) = 0 \qquad (5)$$

Here $\boldsymbol{h} = \boldsymbol{\sigma} \cdot \boldsymbol{n}$ signifies the traction vector.

2.5 Mesh Independence Study

The goal of the mesh independence study is to ensure that the choice of mesh do not affect the accuracy of the results while selecting a model with reduced computing time and resources. Meshing technique of the present study is adopted from study conducted by Sohail *et al.,* [21] using individual inlet edges sizing. Three mesh sizes were examined for each orientation (0, 30, 45, 60 and 90) used in the simulations as shown in Figure 3. Each mesh size presented a similar void fraction, velocity profile and Fast Fourier Transform. Therefore, the FSI simulation's CFD model was employed with intermediate meshes. The FFT and RMS values of pressure fluctuation signal provided a more accurate comparison of the various transient data. FFT involve transferring signal from time to frequency domain, illustrating the distribution of amplitude across frequencies.
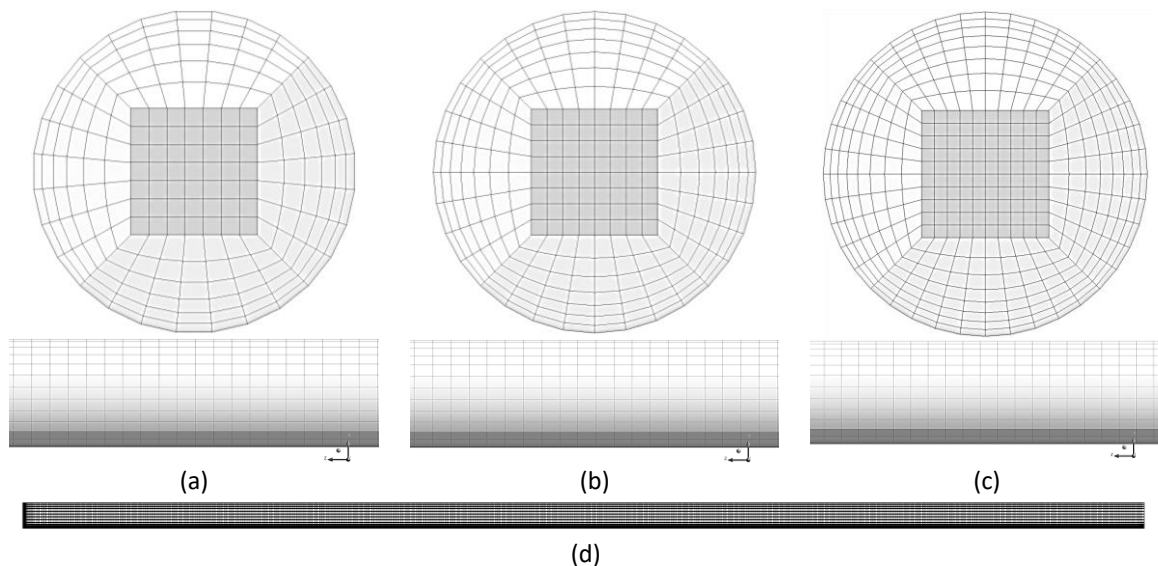
Fig. 3. Side view of inlet and horizontal view showing hexahedral mesh (a) Coarse with 73193 elements, (b) Intermediate with 127189 elements, (c) Fine with 190880 elements, (d) Straight Pipe

The stability and correctness of the numerical solution are greatly influenced by the mesh quality, which is crucial. Skewness, orthogonal quality, and aspect ratio are the criteria used to evaluate the mesh quality. A cell that is equilateral has a value of 0 (best), whereas a cell that is completely degenerate has a value of 1 (worst). Cells with extreme skewness results in an unstable solution.

Skewness value considered for this study was 0.15 to ensure solution stability. The orthogonal quality shows the level of orthogonality of mesh edges. Orthogonal quality of 1 denotes good quality while 0 means inferior orthogonal quality. The average orthogonal quality in the current investigation was 0.97.

Khan *et al.,* [22] discussed the Grid Convergence Index (GCI), that was calculated using Eq. (6), indicates if the results are within the asymptotic range of convergence if the grid resolution gets close to zero. GCI is a scalar indicator for overall numerical solution improvement as mesh is refined [23]. A lower GCI value indicates that numerical solutions produced by using a matching mesh size fall well within the genuine numerical value's range.

$$GCI = \frac{F|\varepsilon|}{(r^p - 1)} \tag{6}$$

$$\varepsilon = \frac{f_2 - f_1}{f_1} \tag{7}$$

$$p = \frac{ln\left(\frac{f_3 - f_2}{f_2 - f_1}\right)}{ln(r)} \tag{8}$$

Factor of safety F, relative error ε, order of convergence p, and selective variables f accumulates these equations for mesh sizing. Number of mesh elements and relative average dynamic pressure are shown in Table 2.

Table 2
Mesh details and convergence criteria

Orientation	Mesh	Elements	Avg. dynamic pressure (KPa)	Grid Convergence Index (%)	Epsilon (m^2/s^3)
0	Coarse	73000	850	1.5	0.06
	Intermediate	127000	980	1.3	0.058
	Fine	190000	1050	1.2	0.055
30	Coarse	73000	950	1.6	0.062
	Intermediate	127000	1020	0.4	0.06
	Fine	190000	1060	1.3	0.058
45	Coarse	73000	1069	1.7	0.064
	Intermediate	127000	1090	1.5	0.062
	Fine	190000	1102	1.1	0.052
60	Coarse	73000	1160	1.8	0.066
	Intermediate	127000	1137	1.6	0.064
	Fine	190000	1130	1.4	0.06
90	Coarse	73000	1250	1.9	0.068
	Intermediate	127000	1185	1.7	0.066
	Fine	190000	1150	1.5	0.065

Simulation is repeated with even finer and with a greater number of elements in mesh until the successive pressure drop tends towards plateau as shown in Figure 4. The selection of this course, intermediate and fine mesh is completely depending on the length of pipe and superficial velocities corresponding to slug flow.
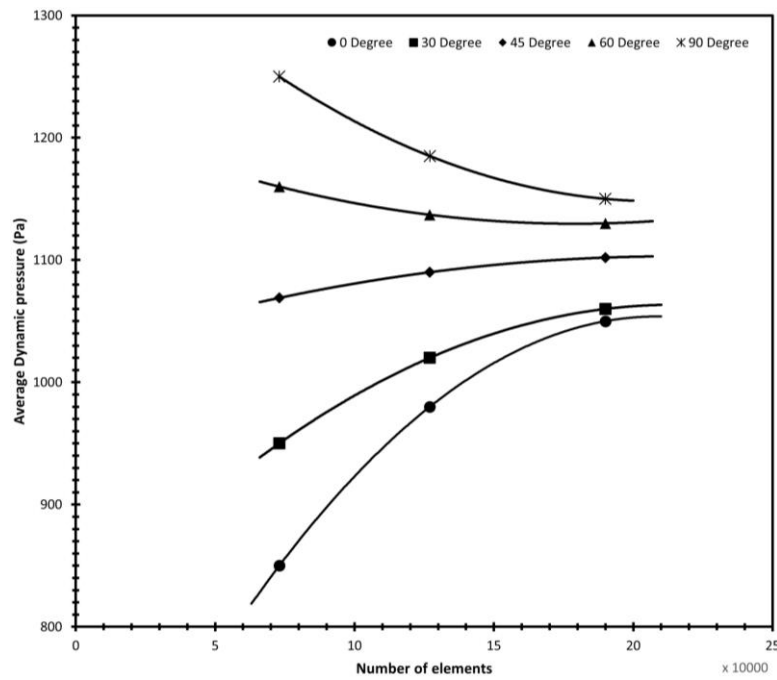
Fig. 4. Grid convergence study for different orientations

3. Results

The coupling model was run for the 0.0525 m pipe and data of 10 s after flow is fully developed and statistically converged. Figure 5 shows the Fast Fourier transforms developed for all studied orientations. Vibration signal at 75D from inlet, collected from transient structure model is processed via FFT and plotted in Figure 6(a) for lateral direction along the. A peak vibrational frequency of 24.4 Hz was obtained for straight horizontal pipe. The effect of gravity was modelled in y-axis for 0-degree inclination. The frequency/amplitude graph is plotted for horizontal piping orientation for the measurement of vibrations in pipe. The last 50 iterations (0.5s) of the flow model are taken and graphed in zoomed part of Figure 3(a). The length of the pipe was 38D, so it was assumed that the flow is fully developed at the end of the pipe. The highest vibration will also occur at this location. It is also observed that the amplitude of frequency is of the scale 0-2.1 of order 10^{-4}. Figure 6(b) shows the Fast Fourier transforms developed for all studied orientations corresponding to y-axis. A peak vibrational frequency of 22.7 Hz was obtained for 60° inclined pipe. The effect of gravity was modelled in x and y-axis for 60° inclination. It is observed that the amplitude of frequency is of the scale 2-10 of order 10^{-5}. It is quite different from the amplitude range of inclined pipes that was observed for x-axis. The reason of this change is orientation and formation of bubbles along the slug flow. The bubble formation is observed as the pipe is inclined greater than 30° which was followed by some medium amplitude and small frequencies of vibrations.
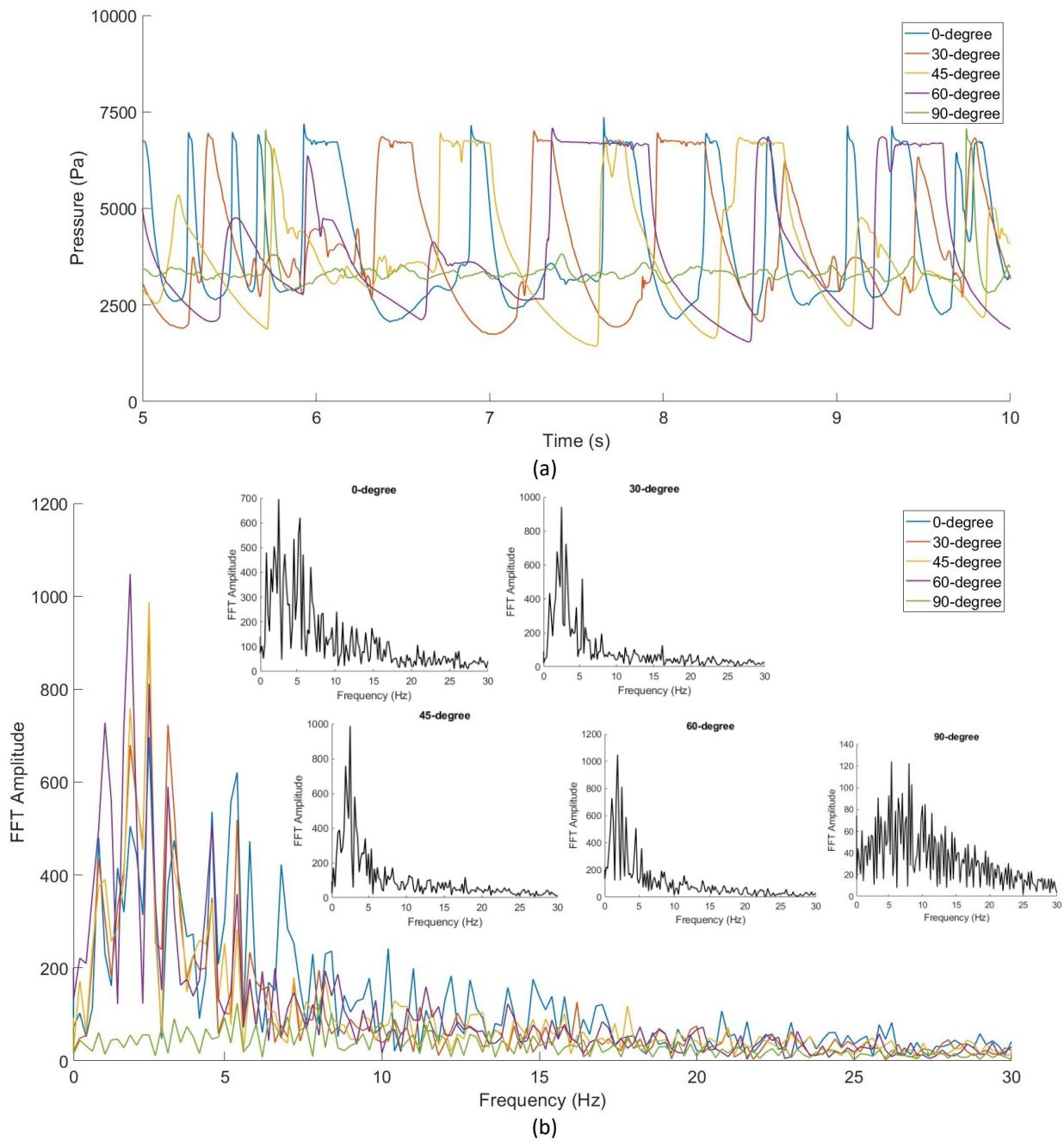
Fig. 5. (a) Pressure vs Time signal comparison for 0, 30, 45, 60, and 90-degree orientations, (b) FFT analysis comparison of pressure signal for the stated orientaions

For the FFT obtained for y-axis it is also observed that there is a significant difference in curves as compared to x and z-axis frequencies. This curve consists of large number of low amplitude and large frequency signals which ultimately shows the impact of slug and bubbles on y-axis of pipe. Figure 6(c) shows the Fast Fourier transforms developed for all studied orientations corresponding to z-axis. A peak vibrational frequency of 24.1 Hz was obtained for 60° inclined pipe. The effect of gravity was modelled in x and y-axis for 60° inclination. There is 7% increase of vibrational frequency along z-axis as compared to y-axis for 60° inclination. When the flow moves from 60° inclination to vertical the formation of slug becomes difficult followed by low frequency peak amplitudes even less as compared to horizontal flow. It is observed that the amplitude of frequency is of the scale 1-4 of order 10^{-6}. Near 90° plane for coarse, intermediate, and fine cases resulted in the maximum pressure at the test section. Minimum pressure was observed for horizontal pipe for slug and annular flow.
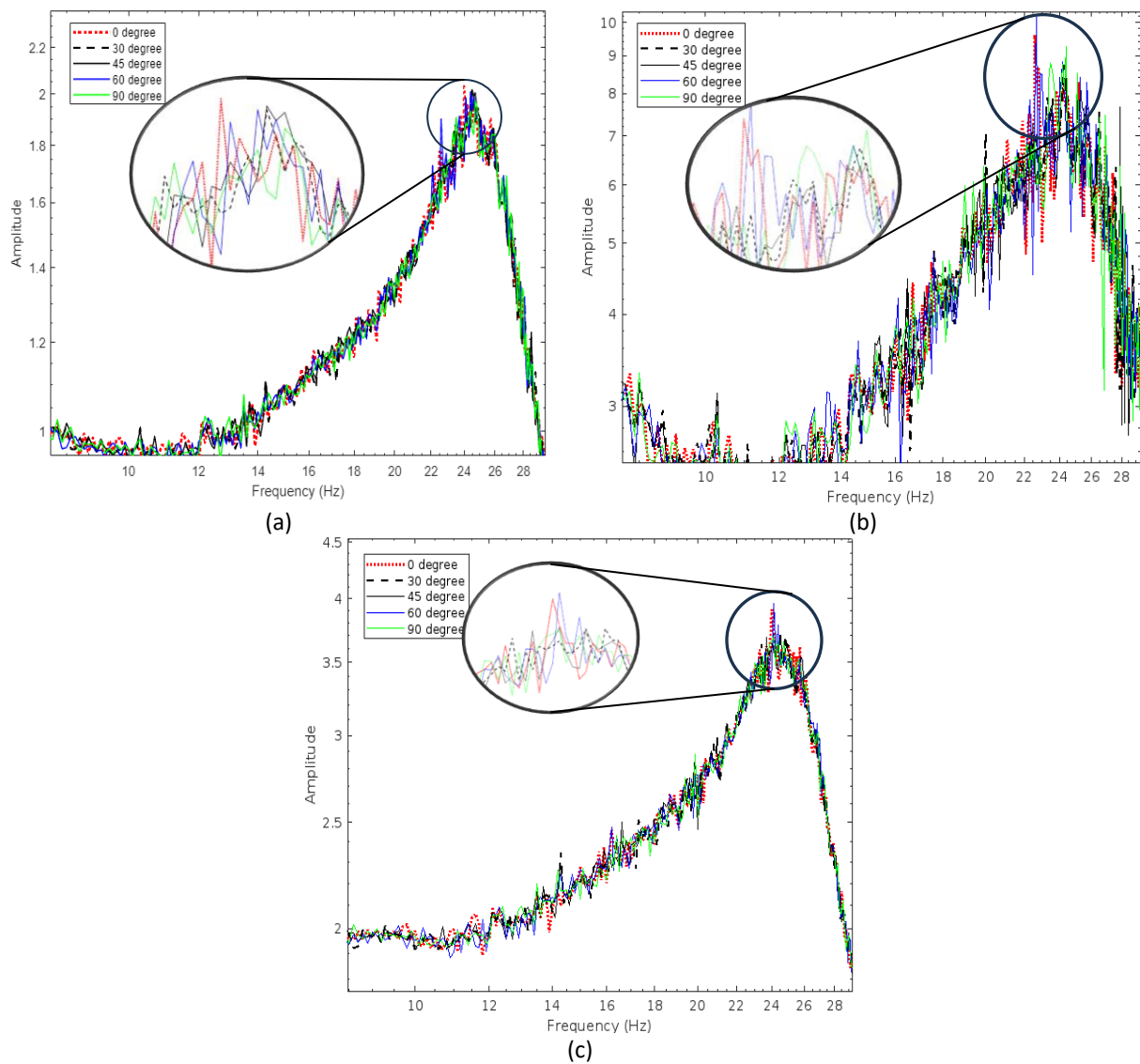
Fig. 6. (a) FFT of x-axis deformation, (b) FFT of y-axis deformation, (c) FFT of z-axis deformation

The deformation data was recorded along the test section of the pipe for 10s after flow is fully developed. Time step of 0.01 was taken for the coupling simulation because the courant number with respect to element size, superficial velocity of air/water and orientation possess a greater impact on the turbulent viscosities along the pipe. The maximum deformations along x-axis and y-axis are shown in Figure 7(a). When the pipe is oriented from horizontal to 45°, the trend in deformation is almost similar but for x-axis it keeps on decreasing and alternatively reverse for y-axis. The deformations are transferred to y-axis despite having different amplitude scale. Finally, the trend that is observed after 45° is inclined towards z-axis in Figure 7(b) and small deformations are observed near 60° orientation.
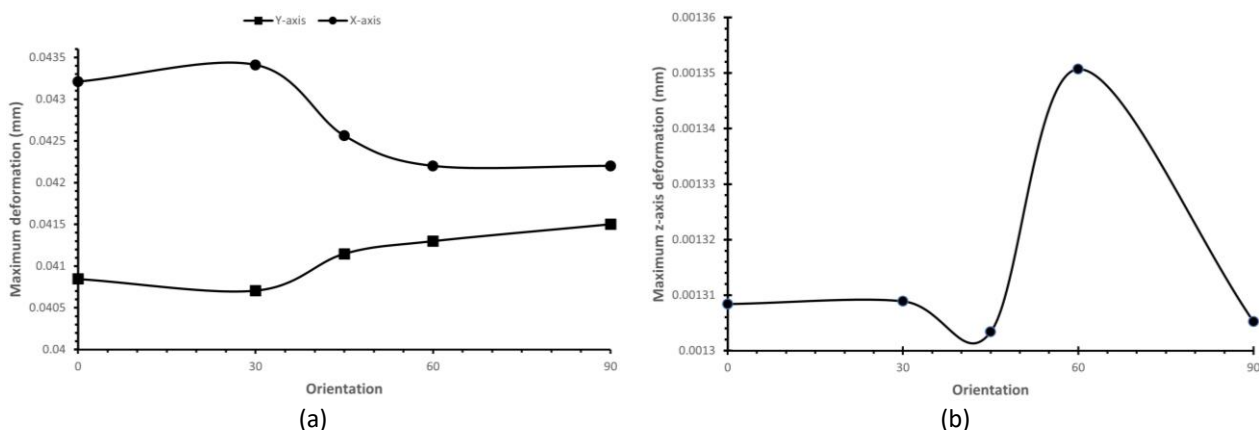
Fig. 7. Maximum deformation along pipe for 0°, 30°, 45°, 60° and 90° inclinations (a) X-axis and Y-axis, (b) Z-axis

4. Conclusions

The amplitude of vibration was maximum for x-axis for all orientations. The displacement magnitude along x-axis increases as we move from 0° to 30° and then decreases till 60° and becomes almost constant when the flow becomes vertical. The highest deformation change is observed between 30°-60° for x-axis and y-axis. 30° possess the highest vibrational deformation in x-axis and lowest in y-axis. Directional velocity for z-axis increases till 45° and then decreases till vertical flow. Maximum directional acceleration of 9 mms^{-2} is observed in 45° orientation. Increment of 7.7% in vibrational frequency is observed for x-axis for 0° - 90° orientations. Y-axis and z-axis show an increase and decrease of 18% vibrational frequency along 0° - 90° orientations.

References
[1] Zheng, X., Z. Wang, M. S. Triantafyllou, and G. E. Karniadakis. "Fluid-structure interactions in a flexible pipe conveying two-phase flow." *International Journal of Multiphase Flow* 141 (2021): 103667. https://doi.org/10.1016/j.ijmultiphaseflow.2021.103667
[2] Ruojun, Qian, Dong Shilin, and Yuan Xingfei. "Advances in research on fluid-structure interaction theory." *Spatial Structure* 14 (2008): 1-13.
[3] Wang, Lin, Yiren Yang, Yuxing Li, and Yating Wang. "Resonance analyses of a pipeline-riser system conveying gas-liquid two-phase flow with flow-pattern evolution." *International Journal of Pressure Vessels and Piping* 161 (2018): 22-32. https://doi.org/10.1016/j.ijpvp.2018.01.005
[4] Yih, T. S., and P. Griffith. "Unsteady momentum fluxes in two-phase flow and the vibration of nuclear system components." In *Proceedings of the International Conference on Flow-Induced Vibrations in Reactor System Components*, pp. 91-111. 1970.
[5] Riverin, J. L., Emmanuel De Langre, and Michel J. Pettigrew. "Fluctuating forces caused by internal two-phase flow on bends and tees." *Journal of Sound and Vibration* 298, no. 4-5 (2006): 1088-1098. https://doi.org/10.1016/j.jsv.2006.06.039
[6] Riverin, J-L., and Michel J. Pettigrew. "Vibration excitation forces due to two-phase flow in piping elements." *Journal of Pressure Vessel Technology* 129, no. 1 (2007): 7-13. https://doi.org/10.1115/1.2388994
[7] Tay, B. L., and R. B. Thorpe. "Effects of liquid physical properties on the forces acting on a pipe bend in gas-liquid slug flow." *Chemical Engineering Research and Design* 82, no. 3 (2004): 344-356. https://doi.org/10.1205/026387604322870453

[8]   Cargnelutti, Marcos F., Stefan PC Belfroid, Wouter Schiferli, and Marlies van Osch. "Multiphase fluid structure interaction in bends and T-joints." In *Pressure Vessels and Piping Conference*, vol. 49231, pp. 75-82. 2010. https://doi.org/10.1115/PVP2010-25696

[9]   Li, Guangzhao, Wenhua Li, Fenghui Han, Shanying Lin, and Xingkun Zhou. "Experimental investigation and one-way coupled fluid-structure interaction analysis of gas-liquid two-phase flow conveyed by a subsea rigid M-shaped jumper." *Ocean Engineering* 285 (2023): 115292. https://doi.org/10.1016/j.oceaneng.2023.115292

[10]   Wang, Zhiwei, Yanping He, Mingzhi Li, Ming Qiu, Chao Huang, Yadong Liu, and Zi Wang. "Numerical Investigation on Dynamic Response Characteristics of Fluid-Structure Interaction of Gas-Liquid Two-Phase Flow in Horizontal Pipe." *Journal of Shanghai Jiaotong University (Science)* (2022): 1-8. https://doi.org/10.1007/s12204-022-2469-7

[11]   De Almeida, Fernando F.M. "Distribuição regional e relações tectônicas do magmatismo pós-paleozóico no Brasil." *Revista Brasileira de Geociências* 16, no. 4 (1986): 325-349. https://doi.org/10.25249/0375-7536.1986325349

[12]   Wang, Alice M., Michael V. Doyle, and David F. Mark. "Quantitation of mRNA by the polymerase chain reaction." *Proceedings of the National Academy of Sciences* 86, no. 24 (1989): 9717-9721. https://doi.org/10.1073/pnas.86.24.9717

[13]   Obradović, Milutin, and Shigeyoshi Owa. "On certain properties for some classes of starlike functions." *Journal of Mathematical Analysis and Applications* 145, no. 2 (1990): 357-364. https://doi.org/10.1016/0022-247X(90)90405-5

[14]   Kvicinsky, Sonia, Florent Longatte, François Avellan, and Jean-Louis Kueny. "Free surface flow: experimental validation of volume of fluid (VOF) method in the plane wall case." In *Proceedings of the 3rd ASME/JSME Joint Fluids Engineering Conference*, San Francisco, CA, USA, July 18-23, vol. 6867. 1999.

[15]   Nichols, B. D., and C. W. Hirt. "Methods for calculating multidimensional, transient free surface flows past bodies." In *Proceedings of the First International Conference on Numerical Ship Hydrodynamics*, vol. 20. Bethesda, MD, USA: Naval Ship Research and Development Center, 1975.

[16]   Hirt, Cyril W., and Billy D. Nichols. "Volume of fluid (VOF) method for the dynamics of free boundaries." *Journal of Computational Physics* 39, no. 1 (1981): 201-225. https://doi.org/10.1016/0021-9991(81)90145-5

[17]   Launder, B. "The numerical computation of turbulent flows." *Computer Methods in Applied Mechanics and Engineering* 3, no. 2 (1974): 269-289. https://doi.org/10.1016/0045-7825(74)90029-2

[18]   Forster, Christiane, Wolfgang Wall, and Ekkehard Ramm. "Artificial added mass instabilities in sequential staggered coupling of nonlinear structures and incompressible viscous flows." *Computer Methods in Applied Mechanics and Engineering* 196, no. 7 (2007): 1278-1293. https://doi.org/10.1016/j.cma.2006.09.002

[19]   Fehn, Niklas, Johannes Heinz, Wolfgang A. Wall, and Martin Kronbichler. "High-order arbitrary Lagrangian-Eulerian discontinuous Galerkin methods for the incompressible Navier-Stokes equations." *Journal of Computational Physics* 430 (2021): 110040. https://doi.org/10.1016/j.jcp.2020.110040

[20]   Donea, Jean, Antonio Huerta, J-Ph Ponthot, and Antonio Rodríguez-Ferran. "Arbitrary L agrangian-E ulerian Methods." *Encyclopedia of Computational Mechanics* (2004).

[21]   Sohail, Muhammad, William Pao, Huzaifa Azam, and Umair Khan. "Two-phase Upward Flow-Induced Vibrations in U-bend under Different Orientations." *Journal of Advanced Research in Fluid Mechanics and Thermal Sciences* 114, no. 1 (2024): 1-12. https://doi.org/10.37934/arfmts.114.1.112

[22]   Khan, Umair, William Pao, and Nabihah Sallih. "Numerical Gas-Liquid Two-Phase Flow Regime Identification in a Horizontal Pipe Using Dynamic Pressure Data." *Applied Sciences* 13, no. 2 (2023): 1225. https://doi.org/10.3390/app13021225

[23]   Marode, Roshan Vijay, Srinivasa Rao Pedapati, Tamiru Alemu Lemma, and Mokhtar Awang. "A review on numerical modelling techniques in friction stir processing: current and future perspective." *Archives of Civil and Mechanical Engineering* 23, no. 3 (2023): 154. https://doi.org/10.1007/s43452-023-00688-6